A combination of rebinning and exact reconstruction algorithms for helical cone-beam CT

Michel Defrise, Frédéric Noo, Hiroyuki Kudo

INTRODUCTION

Cone-beam X-ray transmission computerized tomography (CB-CT) has been applied to the non-destructive evaluation of industrial samples, and a small number of prototype clinical scanners have also been used for specific applications (cardiac and vascular imaging), where fast imaging is an essential requirement and only high contrast structures must be visualized. The recent introduction of multi-row scanners now allows a wide-spread utilization of CB-CT in radiology, and the continuing development of large area x-ray detectors will reinforce this trend.

The acquisition of cone-beam projections allows faster imaging than standard or spiral single-row CT, but presents challenges for 3D image reconstruction. Despite significant advances, the definition of a clinically acceptable, fast and accurate, cone-beam reconstruction algorithm is still an open problem, especially for the helical geometry where the x-ray source moves along a segment of helix relative to the patient. Accurate algorithms for helical CB-CT have been derived by discretizing exact or quasi-exact analytical inversion formulae for the 3D divergent-beam x-ray transform [4,7,8,12]. These algorithms yield accurate reconstructions even when the ratio between the pitch of the helix and the axial slice width exceeds two orders of magnitude. Unfortunately, the numerical complexity of these algorithms significantly increases the reconstruction time and the discretization errors and affects the resolution. These limitations of the exact algorithms motivate an active research for approximate algorithms for helical CB-CT.

In this paper we introduce a new quasi-exact algorithm for the long-object problem in helical CB-CT, which combines a rebinning method with the quasi-exact ZB method [4].

Rebinning algorithms are based on the factorization of the 3D reconstruction into a set of independent 2D reconstructions. This factorization can be viewed as a four-step procedure:

a) *Selection* of a number of 2D surfaces, called *rebinning surfaces*, which partition the 3D field-of-view.

b) *Rebinning*: estimation of a complete 2D tomographic data set (sinogram) for each selected surface using the measured CB projections.

c) *2D reconstruction* of each selected surface from its estimated sinogram.

d) *Axial Interpolation*: 1D interpolation of the reconstructed surfaces to obtain the transaxial slices to be visualized.

Several rebinning algorithms have been proposed, which differ mainly by the type of surface for which rebinned 2D data are estimated. These surfaces can be transaxial slices orthogonal to the axis of the helix [SSRB, 10], tilted planar slices "tailored" to the slope of the helix [9,14,1,3], or even non-planar surfaces as in Heuscher [2] to further improve the possibility to select rays lying as close as possible to the rebinning surface. We present in the following section a unified derivation of the various rebinning methods.

Rebinning algorithms only involve a 1D ramp filtering of the data, and avoid the cone-beam backprojection. This numerical simplicity results in less discretization errors than the exact algorithms. The price to pay for this improvement is that rebinning is approximate and introduces cone-beam artefacts when the pitch of the helix becomes too large.

Therefore, the aim of this paper is to combine the best of the two classes of algorithms: we propose to use a quasi-exact algorithm, the ZB method, to correct a first image reconstructed using a rebinning algorithm. The additive correction is obtained by applying the ZB method to the *residual error*, i.e. to the difference between the measured projections and the cone-beam projections of the first image estimate. This approach is motivated by the fact that the discretization artefacts induced by the exact algorithm only affect the correction image, and hence are expected to be smaller than when the exact algorithm is applied directly to the measured data.

The performance of the combined algorithm is evaluated using synthetic data for mathematical phantoms and for data obtained by reprojecting high resolution CT scans.

M.D. is with the Department of Nuclear Medicine, AZ-VUB, Free University Brussels, Belgium (mdefrise@minf.vub.ac.be).

F.N. is with the Department of Radiology, University of Utah, Salt Lake City (noo@montefiore.ulg.ac.be)

H.K. is with the Department of Information Science and Electronics, University of Tsukuba, Japan (kudo@is.tsukuba.ac.jp)

PLANAR AND NON-PLANAR REBINNING ALGORITHMS

The first contribution of this paper is to give a unified and formal derivation of the various rebinning algorithms which have been proposed in the litterature [1,2,3,9,10,14,15]. We determine the mathematical properties, in particular the symmetries, of the surface allowing the best rebinning, given some reasonable quality figure. This surface is shown to be the solution to an integral equation which can be solved by means of an iterative algorithm. A proof of the convergence of this algorithm and of the unicity of the optimal rebinning surface is given. We also investigate how much can be gained by rebinning onto non-planar surfaces as opposed to planes, and conclude that rebinning onto planar surfaces is sufficiently accurate as long as the radius of the field-of-view does not exceed about half the radius of the helix (figure 1).

For the combined algorithm described in the next section, we rebin on tilted planes, the orientation of which optimize the mean square axial distance Q between the rebinning plane and the measured rays used to build the corresponding 2D data set [3]. We generate a short-scan fan-beam data set rather than a parallel-beam data set, and the mean square axial distance Q is calculated taking into account both the fan-beam redundancy weight (Parker's weight) and the distance dependent weight in the 2D fan-beam backprojection.

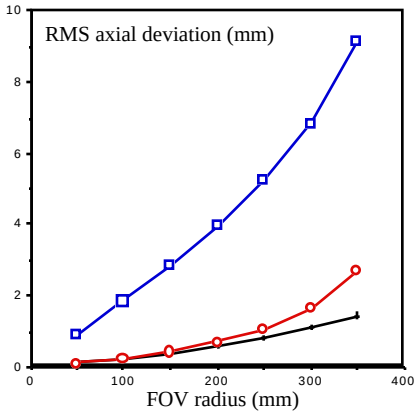

Figure 1: Root mean square axial distance (mm) between the rebinning surface and the measured rays used to build the 2D data set, versus the radius of the FOV (mm). Helix radius 400 mm. Pitch 100 mm. The 3 curves correspond from top to bottom to: SSRB (rebinning on transaxial planes), optimal tilted plane, optimal non-planar surface.

THE COMBINED ALGORITHM

We denote the unknown 3D image by f and the 3D X-ray transform (the CB projector) by X. The data are denoted as $g=Xf$.

Recall first the steps of the ZB algorithm [see 4 for details]:

a) *Weighted backprojection* of the subset of cone-beam data g located, in the detector, along the boundary of Tam's window B[1]. This backprojection operator is denoted X_B^* and is defined so as to yield an image $f_1 = X_B^* g$ the cone-beam projections of which, $g_1 = X f_1$, are equal to the data along the boundary of Tam' window: $g_1 = g$ on ∂B.

b) *Reprojection*: Calculation of the cone-beam projections of the first image estimate f_1 and subtraction from the data to get modified data $g_2 = g - g_1$. Note that $g_2 = 0$ on ∂B.

c) *Reconstruction of the modified data* by

i) setting $g_2 = 0$ outside B,

ii) applying a 1D ramp filter along the direction tangent to the helix,

iii) backprojecting as in Feldkamp's algorithm.

We denote this procedure as $F_{B\text{-}FDK}$ [6] and the result as $f_2 = F_{B\text{-}FDK}\, g_2$.

d) *Addition* of the two images after applying a smoothing filter S designed to match spatial resolutions: $f = S f_1 + f_2$.

The key to the quasi-exactness of the ZB method is the property that $X f_1 = g$ on ∂B. This property is satisfied by the image $f_1 = X_B^* g$ constructed in step *a* above, but this image has no resemblance to the true image f, and therefore the applied correction f_2 (and the associated discretization errors) may be large.

In the combined algorithm proposed in this paper, we build an alternative image f_1 which also satisfies $X f_1 = g$ on ∂B but is in addition a good approximation to f. This is done using a rebinning algorithm (described in the previous section, and denoted by F_{reb}):

a) *Initial reconstruction* by rebinning: $f_{reb} = F_{reb}\, g$

b) *Calculation of a first image estimate* as

$f_1 = X_B^*(g - X f_{reb}) + f_{reb}$

where X_B^* is the weighted backprojection of the data along ∂B, defined above.

The last three steps are as in the ZB method:

c) *Reprojection*: calculation of the cone-beam projections $g_1 = X f_1$ of the first image estimate, and subtraction from the data: $g_2 = g - g_1$

d) *Feldkamp's reconstruction*: $f_2 = F_{B\text{-}FDK}\, g_2$

e) $f = S f_1 + f_2$

One easily checks that the property $X f_1 = g$ on ∂B is satisfied exactly (within discretization errors) by the image $f_1 = X_B^*(g - X f_{reb}) + f_{reb}$ used in this combined algorithm. This guarantees the quasi-exactness of the algorithm. The advantage over ZB is that this f_1 image is a good approximation of the original object, and therefore the correction term f_2, and the associated discretization errors, are

[1] Tam's window B is the region bounded, in the detector, by the cone-beam projection of the upper and lower turns of the helix [11,13].

smaller. The most time consuming steps in the combined algorithm are the calculation of g_1 (step c) and the Feldkamp's step (d).

For the results presented in the following section, we have implemented a simplified version of the algorithm in which we skip step b) and simply use $f_1 = f_{reb}$ instead of $f_1 = X_B^*(g - X f_{reb}) + f_{reb}$. This approximation is motivated by the fact that the image f_{reb} obtained by rebinning may be already sufficiently accurate to guarantee that $X f_{reb} \approx g$ along ∂B. A comparison between the approximate and exact versions of the combined method will be presented at the conference.

RESULTS

We have evaluated the performance of the combined algorithm using simulated data for a head phantom similar to that used by S. Schaller [5]. The phantom is contained in a sphere of radius 100 mm. Data were simulated for a helical path with 1.5 turns and a pitch P=108 mm. The radius of the helix was R=400 mm and there were 1200 vertices per helix turn. The first and last vertices were at locations z=±81 mm. As defined, the helix did not extend over the whole axial extent of the phantom, and we are therefore dealing with a *long object problem*.

Data were simulated on a virtual rectangular detector located at a distance D=400 mm from the cone vertex, i.e. at the isocenter. The detector pixel size was 0.5 x 0.5 mm. There were 400 channels and 200 detector rows.

The angle between the optimal rebinning tilted plane and the transaxial plane was η=3.4 degrees, and the planar rebinning algorithm used the central 134 rows of the detector (maximum cone angle 4.8 degrees). The maximum distance between a ray used for rebinning and the corresponding tilted plane was 2.5 mm, to be compared with 7.8 mm with the SSRB method (η=0). The difference between these two figures illustrates the benefit expected from the planar rebinning algorithms. For all reconstructions, the ramp filter was apodized with a Hamming window cut-off at the Nyquist frequency.

Figures 2, 3 and 4 show reconstructions on a grid of 400x400x200 cubic voxels of 0.5 mm, displayed with a gray scale in the range [1.0,1.1]. The results illustrate the important improvement in image quality obtained by rebinning on tilted planes instead of transaxial planes in SSRB [9,14,1,3]. A reconstruction using optimal non-planar rebinning surfaces (not shown) was practically identical to the reconstruction using tilted planes, as could be expected from figure 1.

The results in figures 2,3,4 also demonstrate that the artefacts observed with the rebinning algorithm are largely suppressed by the combined rebinning-ZB algorithm introduced in this paper. These data also confirm that the short-scan helical Feldkamp (FDK) algorithm (bottom right images) is not superior to planar rebinning, even though FDK uses a "true" cone-beam backprojection.

Figure 5 shows a comparison of the new combined algorithm with the ZB method. Some improvement is observed, especially in the longitudinal section where the streak artefacts caused by the 4 disks are suppressed by the combined method. On the other hand a new artefact is observed around the dark ellipse in the transaxial section. Note that all these results have been obtained with the simplified version of the combined method, as described in the previous section.

A more detailed study using data obtained by reprojecting a high resolution CT scan will be presented at the conference.

REFERENCES

[1] Bruder H, Kachelriess M, Schaller S, Stierstorfer K and Flohr T 2000 Single-slice rebinning reconstruction in spiral cone-beam computetomography, IEEE Trans. Med. Imag.**19** 873-887

[2] Heuscher D 1999 Helical cone beam scans using oblique 2D surface reconstruction. In International Meeting on Fully Three-Dimensional Image Reconstruction in Radiology and Nuclear Medicine, June 23-26 1999, Egmond aan Zee, The Netherlands, 204-207.

[3] Kachelriess M, Schaller S, and Kalender W 2000 Advanced Single-Slice Rebinning in Cone-Beam Spiral CT. Medical Physics 27 754-772

[4] Defrise M, Noo F and Kudo H 2000 A solution to the long object problem in helical cone-beam tomography Phys Med Biol **45** 623-643

[5] Schaller S 1998 Practical image reconstruction for cone-beam tomography PhD thesis, University of Erlangen

[6] Kudo H, Noo F, Defrise M 1998 Cone-beam filtered-backprojection algorithm for truncated helical data Phys Med Biol **43** 2885-2909

[7] Schaller S, Noo F, Sauer F, Tam K C, Lauritsch G, Flohr T 2000 Exact Radon rebinning algorithm for the long object problem in helical cone-beam CT, IEEE Trans. Med. Imag. **19** 361-375

[8] Kudo H, Noo F and Defrise M 2000 Quasi-exact filtered-backprojection algorithm for long-object problem in helical cone-beam tomography IEEE Trans. Med. Imag. **19** 902-921

[9] Larson G L, Ruth C C, and Crawford C R 1998 Nutating slice CT image reconstruction. Patent Application WO 98/44847.

[10] Noo F, Defrise M and Clackdoyle R 1999 Single-slice rebinning method for helical cone-beam CT Phys. Med. Biol. **44** 561-570

[11] Tam K C, Samarasekera S and Sauer F 1998 Exact cone-beam CT with a spiral scan. Phys Med Biol **43** 1015-1024

[12] Tam K C 2000: Exact local regions-of-interest reconstruction in spiral cone-beam filtered-backprojection CT: theory Proc SPIE Med Imag **3979** 506-519

[13] Turbell, H and Danielsson P-E 1998 The PI Method – Non-Redundant Data Capture and Efficient Reconstruction for Helical Cone-Beam CT. Conf. Rec. 1998 IEEE Med. Imag. Conf. (Toronto, Canada)

[14] Turbell, H and Danielsson P-E 1999 An improved PI-method for reconstruction from helical cone-beam projections. Conf. Rec. 1999 IEEE Med. Imag. Conf. (Seattle, WA)

[15] Turbell, H 2001 Cone-beam reconstruction using filtered-backprojection PhD thesis, University of Linkoping

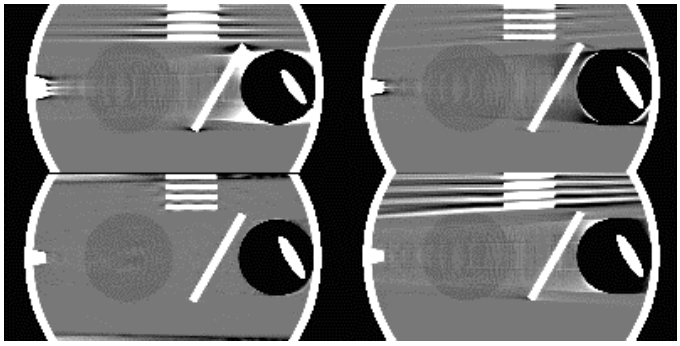

Figure 2. Central longitudinal section x=0. Gray scale [1.0,1.1]. Top left: SSRB, top right: planar rebinning, bottom left: combined rebinning+ZB, bottom right: short-scan FDK.

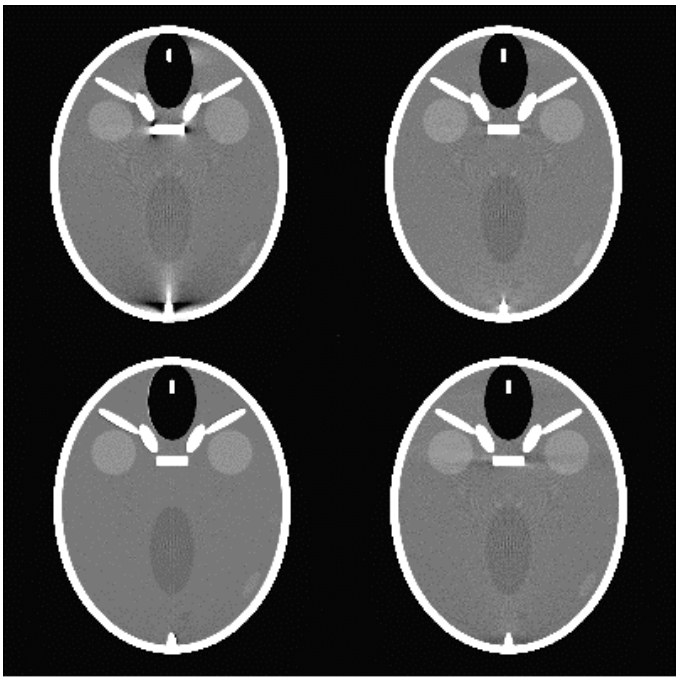

Figure 3. Central transaxial section z=0. Gray scale [1.0,1.1]. Top left: SSRB, top right: planar rebinning, bottom left: combined rebinning+ZB, bottom right: short-scan FDK.

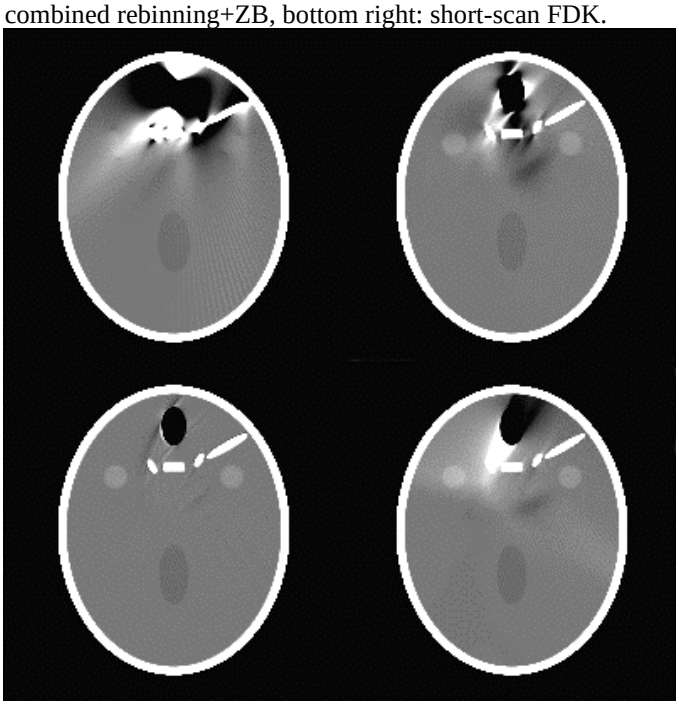

Figure 4. Transaxial section z=19 mm. Gray scale [1.0,1.1]. Top left: SSRB, top right: planar rebinning, bottom left: combined rebinning+ZB, bottom right: short-scan FDK.

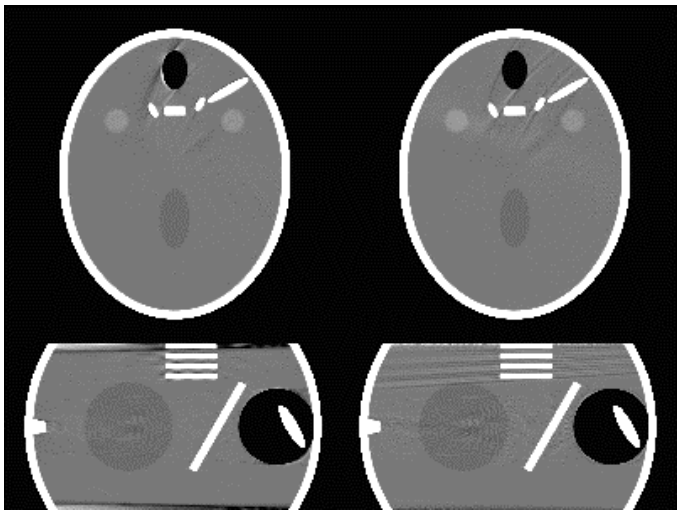

Figure 5. Comparison between the combined method (left column) and the ZB method (right column) for a transaxial section z=19 mm and for a longitudinal section (x=0). Gray scale [1.0,1.1].